JOURNAL OF APPLIED POLYMER SCIENCE VOL. 13, PP. 169–191 (1969)

Structure and Properties of Extruded Polyethylene Film

C. RICHARD DESPER, *U.S. Army Materials and Mechanics Research Center, Watertown, Massachusetts 02172*

Synopsis

A series of low-density polyethylene extruded films was examined quantitatively by the birefringence, infrared dichroism, and x-ray pole figure techniques. The birefringence ranges from mildly positive to mildly negative with increasing severity of quenching conditions. The x-ray data show that the birefringence is largely due to the contribution of oriented crystallites, the amorphous orientation being quite low. The crystal orientation functions suggest equal degrees of *a* and *c* axis orientation parallel to the machine direction at low quenching rates, and increasing *a* axis orientation as the quenching rate increases, coupled with a shift in the *c* axis from parallel to perpendicular orientation. These results are confirmed by infrared dichroism data. The relative degree of *a* and *c* axis orientation ultimately reached is intermediate between that predicted by Keller's type I and type II models, but approximates the orientation previously observed in laboratory films prepared by oriented crystallization at 100% elongation. The crystalline orientation may be explained by the modified row orientation structure of Keller and Machin. However, the data can also be reconciled with that of spherulitic entities observed in samples crystallized at 20–50% stretch. It is suggested that these spherulites may possess a combination type II and screw dislocation morphology in the equatorial and polar regions, respectively. Such a structure differs from the row structure in that the latter implies that the amount of polar material is negligible compared to the equatorial material. It is recognized, however, that orientation data cannot unambiguously decide between these alternatives.

INTRODUCTION

The production of tubular extruded polyethylene film, or "blown" film, is a common industrial process which results in preferred orientation. The type of orientation obtained has been a topic of concern and controversy over a period of years. No attempt will be made to survey the literature in great depth, since recent publications by Lindenmeyer and Lustig[1] and by Keller and Machin[2] cover the subject quite well. The orientation is generally presumed to arise from a process of oriented crystallization. As the molten polymer is extruded to form a film, orientation is produced in the hot, amorphous material by the action of a longitudinal velocity gradient. The material subsequently crystallizes from the oriented melt, the morphology produced being profoundly affected by the amorphous orientation.

The crystallization process stiffens the polymer sufficiently to prevent much further deformation. Support for this sequence of events may be adduced from the fact that types of orientation quite similar to those found in blown films may be obtained upon crystallization of a crosslinked, oriented melt at fixed extension.[3–6]

In general, extruded films are found to crystallize with the *a* axis oriented parallel to the machine direction and the *b* axis perpendicular. The same is true of oriented crosslinked melts crystallized below about 200% elongation. Recent work by Kitamaru and co-workers[7] indicates that in the latter case the material with parallel *a*-axis orientation may be, in fact, polymer which failed to crosslink, since the effect is not observed when such material is removed by solvent extraction prior to crystallization. This would suggest that, in the film extrusion process, the amorphous, oriented matrix in which crystallization occurs is more like a partially crosslinked system, with many polymer chains not participating in the network. The longest molecules are more likely to form entanglements which act as temporary crosslinks, leaving the shorter molecules relatively free to disorient. Holmes and Palmer[8] found, in some instances, that the *a* axis was tilted at an angle to the machine direction. While this behavior is unusual, it has also been observed in oriented, crosslinked polyethylene crystallized at higher elongations.[4–6]

Lindenmeyer and Lustig[1] have pointed out that merely qualitative knowledge of the *a*- and *b*-axis distributions may lead to erroneous conclusions concerning the *c*-axis distribution. To avoid this pitfall, they measured the *c*-axis distribution directly, using the weak (002) reflection. This was ruled out in our case because of the low degree of crystallinity of the samples, which resulted in a very low (002) intensity. Instead, we chose to obtain quantitative data on the (200) and (110) orientation distributions to calculate orientation functions for the *a*, *b*, and *c* axes.

The method of data analysis has been fully described in the literature.[6] Three functions, $\langle \cos^2\phi_{hkl,\,x} \rangle$, $\langle \cos^2\phi_{hkl,\,y} \rangle$, and $\langle \cos^2\phi_{hkl,\,z} \rangle$ are used to characterize the orientation of the (*hkl*) diffraction plane with respect to the major axes (*xyz*) of the sample. For the orthorhombic crystal system, only two (*hkl*) planes will have independent orientation functions. This fact arises from the symmetry of the unit cell; no assumptions concerning the nature of the orientation distributions are involved. Consequently, with accurate data on only two diffraction planes [such as (110) and (200)], the orientation functions of any crystallographic direction (such as the *c* axis) may be computed. This is not to imply that we know the *c*-axis distribution; data from many more diffraction planes would be required to solve for the *c*-axis distribution. We merely know certain second-order averages of the *c*-axis distribution. The value of orientation functions is enhanced, however, by the fact that certain properties (e.g., birefringence and infrared dichroism) depend only upon these orientation functions, not upon the entire distributions. Thus, the orientation function approach affords an opportunity for crosscorrelation between several independent experiments.

EXPERIMENTAL AND RESULTS

X-Ray Diffraction

A series of tubular extruded films was provided by P. J. Grey of Monsanto Chemicals, Ltd. Results of light-scattering experiments with two of these films were previously reported.[9] The conditions of preparation are shown in Figure 1 and tabulated in Table I. The samples were extruded as a tube from an annular ring die, inflated by an internal air bubble, and drawn away from the die by a pair of nip rollers. The hot polymer deforms in two directions (machine and transverse) prior to solidification, so the stress history is not purely uniaxial. The deformation ratio in the machine direction is the ratio of takeup velocity to melt velocity at the die and was set at 7 for these samples. The true deformation ratio in the transverse direction was 1.52–1.64 for these samples, so the deformation was considerably greater in the machine than in the transverse directions. Cooling air was blown over the emerging polyethylene from a slotted ring encircling the die. The takeoff speed, melt temperature, film thickness, polymer flow rate, and blowup ratio were held constant or nearly so. The cooling air velocity varied in a monotonically increasing fashion from the first sample (32A) to the last (32G). The internal bubble pressure was increased concurrently to maintain a nearly constant blowup ratio.

Samples of three blown films were prepared for x-ray pole figure determination by gluing together twenty thicknesses of film for each sample. The pole figures obtained for the three samples are shown in Figures 2–4, and the orientation functions are plotted in the XYZ triangular plot in Figure 5. The methods used for obtaining the pole figures and for plotting the orientation functions were previously described.[6]

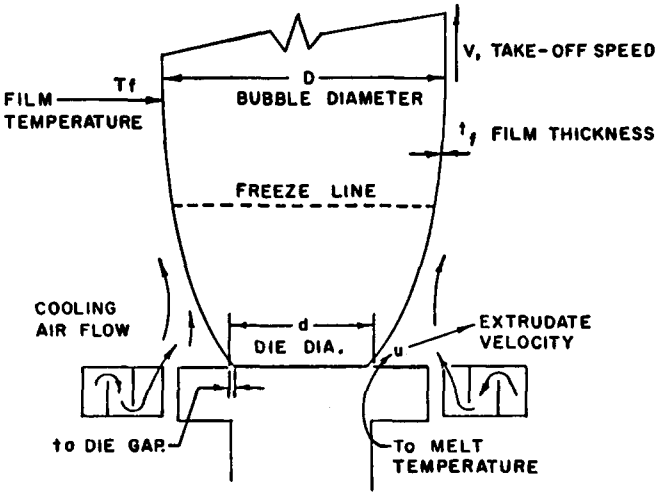

Fig. 1. Tubular film extrusion process.

TABLE I
Conditions of Manufacture of Tubular Extruded Polyethylene Films[a]

Sample	Cooling air velocity, in H_2O pressure drop in pitot tube	Internal bubble pressure, in. H_2O	Thickness, in.	Blow-up ratio[b]	True transverse deformation ratio
32A	0.075	0.085	0.00095	2.58	1.64
32B	0.10	0.115	0.0008	2.52	1.61
32C	0.20	0.175	0.0008	2.48	1.58
32D	0.35	0.30	0.0009	2.44	1.55
32E	0.50	0.475	0.0009	2.44	1.55
32F	0.70	0.68	0.0010	2.40	1.53
32G	0.80	0.82	0.0009	2.38	1.52

[a] For all samples: takeup velocity V_f = 27 ft/min; velocity ratio V_f/u = 7; melt temperature T = 350°F (177°C); resin type: low-density (0.92 g/cm³).

[b] Defined as the ratio of the width of the flattened film tube to die diameter in accordance with established practice. Thus a film with a true transverse deformation ratio of 1 would have a "blow-up ratio," as conventionally defined, of $\pi/2$ or 1.57.

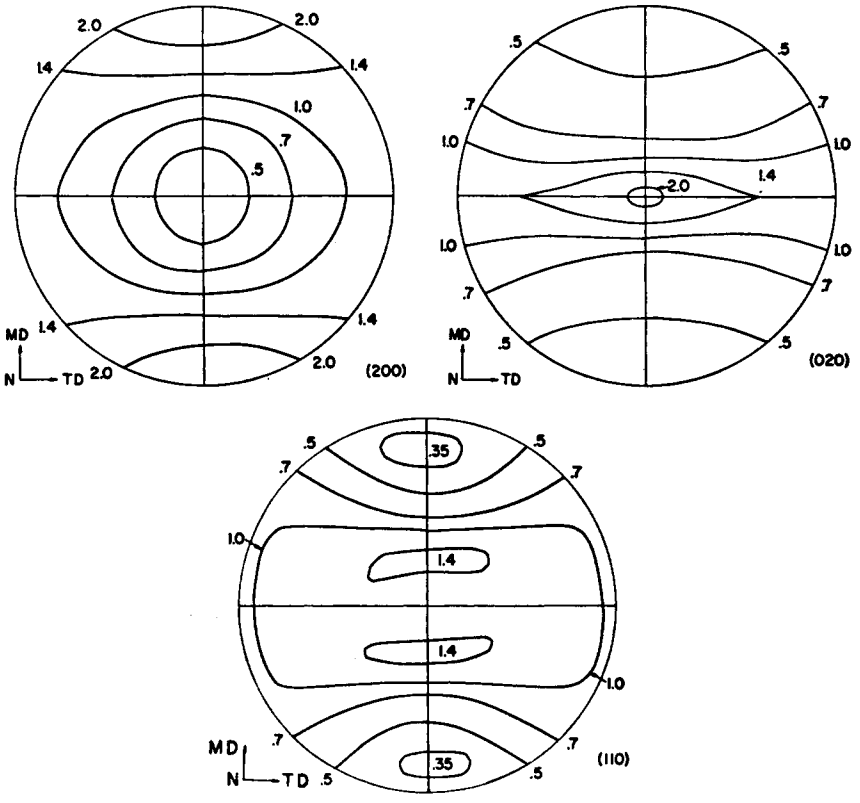

Fig. 2. Pole figures of sample 32A.

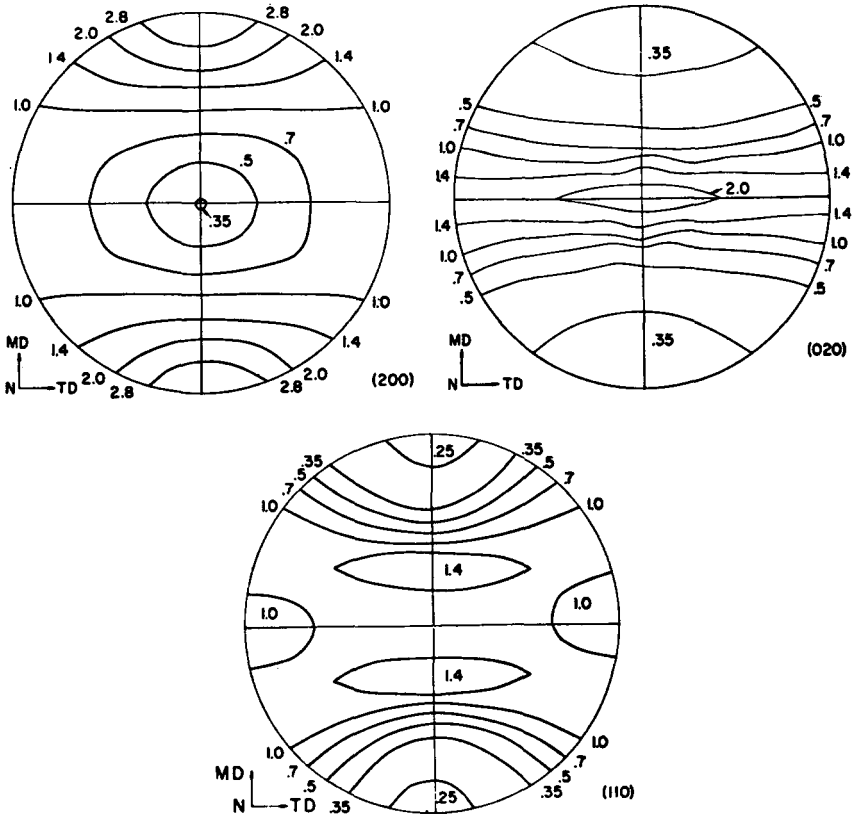

Fig. 3. Pole figures of sample 32B.

The pole figures show both internal consistency within a given sample and progressive changes from sample to sample. For 32A, the distribution of the *a* axis shows a maximum in the machine direction, intermediate intensity in the transverse direction, and a minimum in the normal direction. Conversely, the *b* axis distribution shows a maximum in the film normal direction and a minimum in the machine direction. The (110) pole figure corroborates the other two. The (110) poles are found to concentrate in a belt at an angle of approximately 60° to the machine direction. However, the distribution is not uniaxial; the highest contour lines are two islands located where this belt approaches nearest to the film normal direction. Since the (110) normal lies in the *ab* plane at an angle of 57° from *a*, the locations of these (110) maxima are consistent with the *a*- and *b*-axis distributions.

Proceeding to 32B, the three pole figures are similar to the corresponding pole figures for 32A. The same features appear; the differences are quantitative rather than qualitative. The (110) pole figure is practically unchanged, but the *a*- and *b*-axis distributions have become sharper, as indicated by the appearance of additional contour lines. In sample 32G,

marked changes are seen. The pole figures show only slight deviations from cylindrical symmetry. The b axis maximum at the film normal and the (110) "islands" have dwindled to nearly nothing. In the a-axis pole figure, only the lowest intensity contour lines show deviations from cylindrical symmetry, and these deviations are of little importance.

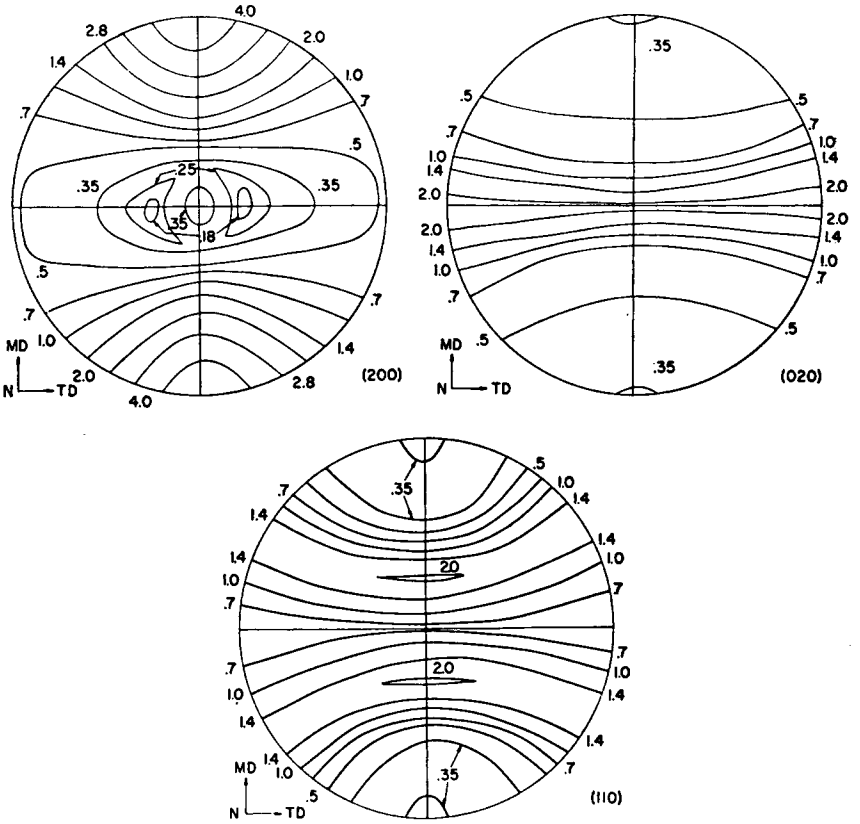

Fig. 4. Pole figures of sample 32G.

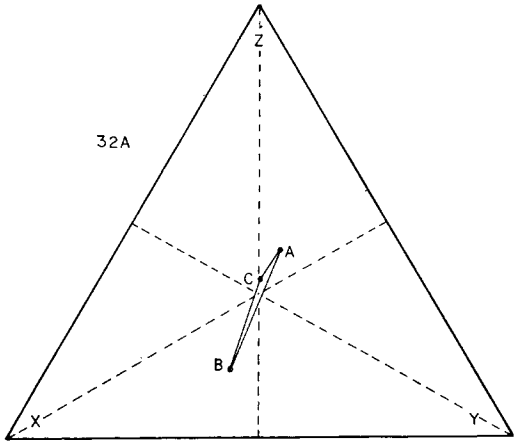

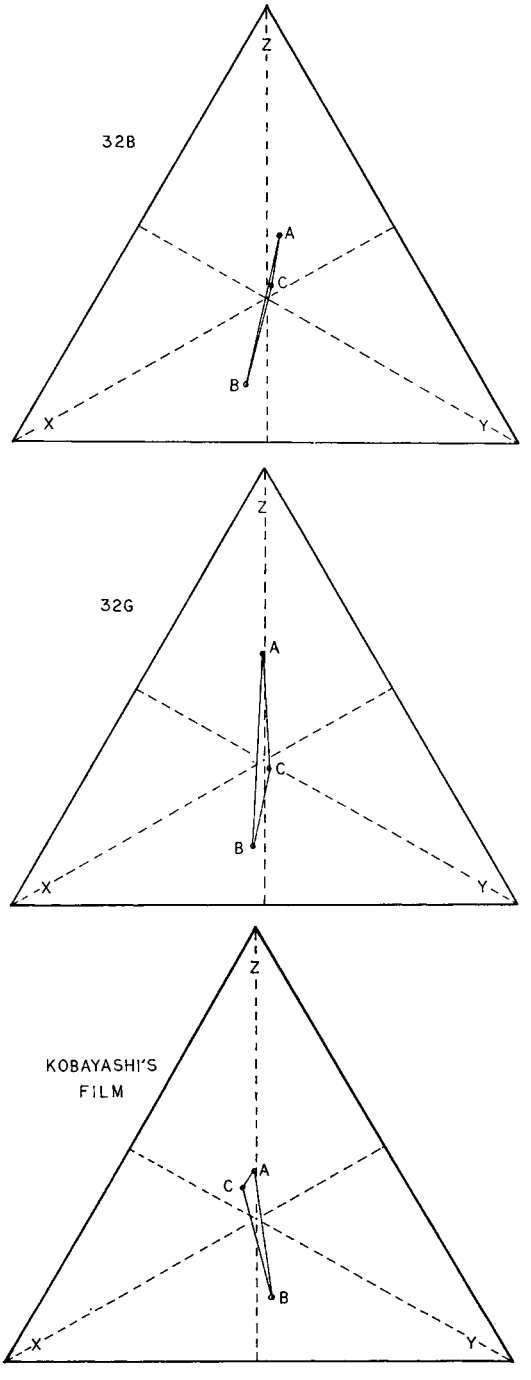

Fig. 5. Orientation functions of extruded films shown on the XYZ equilateral triangle plot. Coordinate system: X = film normal, Y = transverse direction, Z = machine direction. Data also shown for a high density extruded film kindly supplied by K. Kobayashi.

The tendency for b-axis orientation towards the film normal, seen in 32A and 32B, is probably a result of preferential nucleation at the surface of the film. Presumably, growth of crystallites starts at a larger number of growth centers on the film surface. Due to impingement of these crystallites on each other, they are forced to grow mainly in the film normal direction, other avenues of growth being blocked. The growing crystals advance into the interior of the film in a planar front, forming a skin on the film. This phenomenon, often called "transcrystallization," has been observed by numerous workers.[10-13] Since growth is in the crystallographic b direction the net result is orientation of the b axes toward the film normal. The effect is presumably suppressed in 32G by fast quenching.

These pole figures may be compared with data previously published by Lindenmeyer and Lustig.[1] Their pole figures for low-density resins at blow ratios of 3.3 and 6.7 are somewhat similar to those of 32A; however, Lindenmeyer and Lustig found a greater degree of b-axis orientation. Sample 32G shows much more a-axis orientation and much less b-axis orientation than any of the low density films investigated by Lindenmeyer. A comparable degree of a-axis orientation is found in one of their high-density films (blow ratio 6.7).

The orientation functions plotted in Figure 5 were calculated from the orientation functions of the two most intense reflections, (110) and (200), as previously described.[6] As we proceed in the sequence 32A, 32B, and 32G, the a- and b-axis orientation functions approach the altitude of the triangular plot, which is the locus for uniaxial orientation about the machine direction (Z). Increasing a axis orientation towards Z is indicated by movement of point a on the plot closer to the Z vertex.

Of greatest interest, however, is the behavior of the c-axis orientation functions, since the c-axis distribution cannot be determined by direct measurement in these low-density samples. The c axis point starts above the center of the triangular plot for 32A. For 32B, point c is lower and for 32G is has dropped below the center point. This indicates a change in the sign of $f_{c,Z}$ from positive to negative and a corresponding change in $\Delta_{c,x}$, the crystalline portion of the birefringence Δ_x measured at normal incidence. There is a concurrent shift in the observed birefringence Δ_x from positive to negative.

Although we cannot describe the c-axis distribution from knowledge of its orientation functions, we can rule out distributions which are inconsistent with the observed values. For instance, Lindenmeyer and Lustig determined the c-axis distributions for four high-density samples by use of the weak (002) reflection. Three of these distributions show nearly uniaxial distribution of the c axis, with a mild maximum in intensity at the machine direction. The pattern would be characterized by a positive value of $f_{c,z}$ and thus is consistent with the data of sample 32A. This pattern may be ruled out for sample 32G, however, because of the sign of $f_{c,z}$. Despite the qualitative similarity between our a- and b-axis pole figures and those of Lindenmeyer, there is a subtle difference which is apparent upon quantita-

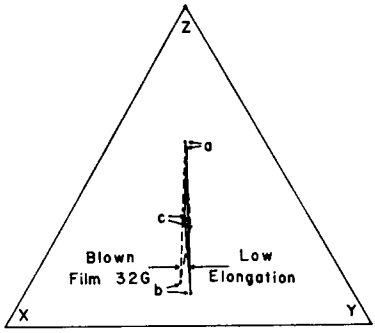

Fig. 6. Comparison of orientation functions: extruded film 32G and a sample crystallized at 100% elongation.

tive examination of the data. Our data for 32G shows a high degree of a-axis orientation, as high as any found by Lindenmeyer, but much milder b-axis orientation. The difference is enough to shift the c-axis orientation functions from positive to negative.

It is interesting to compare the pattern of orientation in 32G with recently published data[6] obtained by oriented crystallization of crosslinked polyethylene. The sample in question was crosslinked with high-energy radiation, melted, stretched 100%, and cooled to 104°C. The pole figures for the two samples are in almost quantitative agreement. The orientation functions are plotted in Figure 6 and are remarkably similar. Most likely, the structure of the two samples are also similar.

Birefringence Measurements and Calculations

Birefringence measurements and calculations were used to confirm the results obtained by x-ray diffraction and to obtain a measure of the state of amorphous orientation. Two birefringence values were obtained for each of the low density films:

$$\Delta_x = n_z - n_y \tag{1}$$

which is the usual birefringence measured at normal incidence, and

$$\Delta_y = n_z - n_x \tag{2}$$

Birefringence was measured on a polarizing microscope using a Berek compensator. Since it was necessary[14] to tilt the samples away from normal incidence to measure Δ_y, the sample was mounted between glass hemispheres ($n = 1.516$) on a universal stage to minimize refraction at the sample surface. This improves the accuracy of the Δ_y determination.[15] Although examination at the highest magnifications with the polarizing microscope revealed no resolvable structure, birefringence data were obtained at lowest magnification to average over a larger area of sample.

The crystallite contribution to Δ_x and Δ_y was calculated from (110) and (200) orientation functions, and the amorphous contribution was found by

TABLE II
Measured and Calculated Birefringence Values

	Blown films			Oriented crystallization	
	32A	32B	32G	100%	200%
In-plane birefringence (measured at normal incidence)					
$x_{c,V}$[a]	0.460	0.426	0.426	0.41	0.38
Δ_x	0.0023	0.0016	−0.0032	−0.002	0.0186
$\Delta_{c,x}$	0.0044	0.0025	−0.0063	0.0048	0.0300
$\Delta_{A,x}$	0.0004	0.0009	−0.0010	−0.0037	0.0015
Out-of-plane birefringence					
$x_{c,v}$[a]	0.460	0.426	0.426	0.41	0.38
Δ_y	0.0045	0.0049	0.0008	b	0.0235
$\Delta_{c,y}$	0.0054	0.0042	−0.0035	0.0005	0.0185
$\Delta_{A,y}$	0.0037	0.0054	0.0052	b	0.0266

[a] Volume fraction crystallinity determined from density measurements.
[b] Measurement not possible due to great thickness of sample.

difference. The procedures used have been previously described.[6] The results of these calculations are shown in Table II, along with previously published data on two films prepared by oriented crystallization. The quantities listed are related by:

$$\Delta_x = x_{c,V}\Delta_{c,x} + (1 - x_{c,V})\Delta_{A,x} \tag{3}$$

and

$$\Delta_y = x_{c,V}\Delta_{c,y} + (1 - x_{c,V})\Delta_{A,y} \tag{4}$$

The in-plane birefringence Δ_x is positive for 32A, decreases with 32B, and becomes negative for 32G. This trend is duplicated almost quantitatively in the calculated values of the crystalline contribution to Δ_x, leaving only a small contribution attributable to amorphous orientation. In contrast, the out-of-plane birefringence Δ_y is positive for 32A and 32B, and becomes negative for 32G. The calculated amorphous contribution to Δ_y is positive for all three samples, and is considerably greater than the amorphous contributions to Δ_x. Thus, the amorphous birefringence is nearly uniaxial in character, with the film normal being the symmetry axis. The near-zero values of $\Delta_{A,x}$ indicate that the "balanced film" condition has been nearly achieved as far as the amorphous chains are concerned. The positive values of $\Delta_{A,y}$ indicate preferential orientation of the amorphous chains parallel to the plane of the film. (It is notable that the x-ray data shows a slight tendency for the chains in the crystalline regions as well to orient parallel to the plane of the film). The values of $\Delta_{A,x}$ and $\Delta_{A,y}$ are considerably lower for the blown films than for the "oriented crystallization" samples. The explanation for this probably lies in the fact that the "oriented crystallization" samples were crosslinked. These crosslinks impose

TABLE III
Comparison of $\Delta_{c,x}$ and $\Delta_{c,y}$ Values Obtained by Rigorous and Approximate Methods of Calculation[a]

Sample	$\Delta_{c,x}$		Error,	$\Delta_{c,y}$		Error,
	I	II	%	I	II	%
32A	43.8	51.4	17	53.5	66.1	24
32B	25.4	36.3	43	41.7	56.1	35
32G	−62.8	−47.1	25	−34.6	−17.8	49

[a] I = rigorous method. $\Delta_{c,x} = (n_c - n_a)(\langle\cos^2\phi_{c,z}\rangle - \langle\cos^2\phi_{c,y}\rangle) + (n_b - n_a)(\langle\cos^2\phi_{b,z}\rangle - \langle\cos^2\phi_{b,y}\rangle)$. II = Approximate method. $\Delta_{c,x} = (n_c - \frac{1}{2}[n_a + n_b])(\langle\cos^2\phi_{c,z}\rangle - \langle\cos^2\phi_{c,y}\rangle)$.

restraints upon the amorphous chains which are not present in the blown films. Consequently, relaxation of the orientation of the amorphous regions is less complete in the crosslinked films.

The crystal contribution to birefringence shows significant biaxial character in all three samples. However, one must be careful in interpreting the crystal birefringence. In polyethylene, the values of $\Delta_{c,x}$ and $\Delta_{c,y}$ are sensitive mainly to the c-axis orientation, and birefringence values are often thought of as being dependent upon the c-axis distribution alone. Such an approximation would be exact if n_a and n_b were equal for polyethylene crystals, or if the orientation functions for the a and b axes were equal for the sample in question. However, for these blown films, in which the a- and the b-axis distributions are completely different from each other, the difference between n_a and n_b must be taken into account in calculating $\Delta_{c,x}$ and $\Delta_{c,y}$. Table III shows that the error one would incur by assuming n_a and n_b to be equal ranges from 17% to 49% for these samples. Two conclusions are apparent: (1) one must be careful when calculating crystalline birefringences for blown films, and (2) having calculated $\Delta_{c,x}$ and $\Delta_{c,y}$ correctly, one must be wary of interpreting the results in terms of c axis orientation alone.

Infrared Dichroism Measurements and Calculations

The following infrared absorption bands were used to characterize the orientation of the blown films: the CH_2 rocking doublet at 722–733 cm^{-1}, two amorphous bands at 1300 and 1380 cm^{-1}, the CH_2 bending doublet at 1468–1480 cm^{-1}, and two weaker bands (1903 and 2030 cm^{-1}) which are regarded as combination or overtone bands.[16] For both of the doublets the higher-frequency component is absorbed in the crystalline regions only and the dipole moment change vector **M** is along the a axis,[17] so the dichroisms of these peaks are measures of the a-axis orientation functions. The lower frequency components of the doublets are of little use because they are absorbed in both amorphous and crystalline regions, however, their presence limits the accuracy in the measurement of the intensities of the high frequency components. The dipole moment change for the 1300 and

1380 cm^{-1} amorphous bands is parallel to the chain backbone direction. Although the nature of the 1903 and 2030 cm^{-1} bands is not entirely clear, several facts have been established: (a) the 1903 cm^{-1} band is of purely crystalline origin and, in fact, has been used[18] to measure crystallinity; (b) the 2030 cm^{-1} band is absorbed in both crystalline and amorphous regions;[16] and (c) highly stretched samples are found[17,19,20] to exhibit very high perpendicular and parallel dichroism for the 1903 and 2030 cm^{-1} bands, respectively. For the 1903 cm^{-1} band **M** must be perpendicular to *c*, but the location of **M** in the *ab* plane is thus far not known. The results of these experiments will, in fact, clarify the question of the location of **M** for this particular absorption. The 2030 cm^{-1} band is assigned to *trans* configurations[19] in both amorphous and crystalline regions,[21] with **M** parallel to the chain backbone and thus parallel to *c* in crystalline regions.

In order to measure the dichroism of both the strong and the weak bands two sample thicknesses were used. The spectra of thin samples (0.002 in.) were obtained by using a Perkin-Elmer 621 spectrophotometer, while spectra of thicker specimens (0.018 in.) were obtained with a Beckman IR-12. The polarizer was a Perkin-Elmer wire grid type which has negligible transmission for the unwanted component. Since the thicker samples consisted of eighteen separate films, hexafluorobutadiene was used between layers as an immersion fluid to reduce reflection losses. To avoid error due to instrument polarization, the sample was rotated instead of the polarizer.

Methods have been described[19] for obtaining A_X, A_Y, and A_Z, the absorbancies for radiation polarized along the corresponding sample directions. Due to lack of a suitable apparatus the A_X measurement was not made; the data are expressed in terms of R_{ZY}, the ratio of A_Z to A_Y. The experimental ratios are compared in Table IV with calculated values. For the purely amorphous bands at 1300 and 1380 cm^{-1}, a value of R_{ZY} of about 1

TABLE IV
Measured and Calculated Infrared Dichroism Values

			R_{ZY}			
			32A		32G	
ν, cm^{-1}	Direction of M[a]		Experimental	Calculated	Experimental	Calculated
722	$A(\perp)$	$C(b)$	0.6	—	0.6	—
733	$C(a)$		1.5	1.3	2.5	2.5
1300	$A(\parallel)$		1.0	≈1	1.1	≈1
1380	$A(\parallel)$		1.0	≈1	1.0	≈1
1468	$A(\perp)$	$C(b)$	0.6	—	0.4	—
1480	$C(a)$		1.3	1.3	2.5	2.5
1903	$C(\perp)$		0.94	—	1.36	—
2030	$C(c)$	$A(\parallel)$	1.2	1.3	0.8	0.8

[a] A = amorphous, C = crystal, a, b, c = crystallograhic axes, $\parallel$ = paralell to chain; and $\perp$ = perpendicular to chain.

is predicted, based on the low values calculated for $\Delta_{A,x}$. For the a axis bands, R_{ZY} should be given by:[6]

$$R_{ZY}(a) = \langle\cos^2\phi_{a,z}\rangle/\langle\cos^2\phi_{a,y}\rangle. \quad (5)$$

These values are compared in Table IV with dichroisms measured at 733 and 1480 cm^{-1}. The dichroism at 2030 cm^{-1} is compared with values calculated from the crystalline c-axis orientation functions:

$$R_{ZY}(c) = \langle\cos^2\phi_{c,z}\rangle/\langle\cos^2\phi_{c,y}\rangle \quad (6)$$

The equation admittedly neglects the contribution of amorphous regions to the band at 2030 cm^{-1}; nonetheless, the calculated and experimental values were in good agreement.

Several previous conclusions were confirmed by the infrared data: (a) the degree of a axis orientation increases markedly between samples 32A and 32G; (b) the c-axis orientation shifts from mildly parallel to mildly perpendicular; (c) the state of amorphous orientation is low.

The comparison may also be shown in terms of the ternary orientation function diagram. It has been shown[22] that lines of constant R_{ZY} can be mapped onto the diagram as straight lines emanating from the X vertex. Lines of constant dichroism are shown in Figures 7 and 8 for the various experimentally determined R_{ZY} values. For the a-axis bands the lines come reasonably close to the points obtained by x-ray diffraction. The dichroism at 2030 cm^{-1} also appears to follow the c-axis data point, determined by x-ray diffraction, despite the unknown effect of amorphous orientation at this frequency.

For comparison, Aggarwal and co-workers[23] measured the dichroism of ten extruded films at 733 cm^{-1} and obtained values in the range 1.1–2.5. Their highest value corresponds to the value for sample 32G, indicating comparable degrees of a axis orientation. The value 2.5 is also higher than the limiting value of 2.0 calculated by Keller and Sandeman[24] for the row orientation structure.

Of particular interest, however, is the behavior of the 1903 cm^{-1} band, since we have no way of knowing where **M** is located within the unit cell, other than knowing that it lies in the ab plane. Since the a and b axis orientation functions are widely separated, these experiments afford an opportunity for estimating the location of this **M** vector. We know that the orientation functions governing this absorption must lie on two lines: the line ab and the experimental constant R_{ZY} line. The intersection of these lines in Figures 7 and 8 are denoted M. The lengths of the line segments $\overline{Ma}$ and $\overline{Mb}$ can be used to calculate the position of M in the ab plane. We may write:[6]

$$\overline{Ma}:\overline{Mb} = \cos^2\phi_{M,b}:\cos^2\phi_{M,a} \quad (7)$$

From this we obtain

$$\cos^2\phi_{M,a} = \overline{Mb}/(\overline{Ma} + \overline{Mb}) = \overline{Mb}/\overline{ab} \quad (8)$$

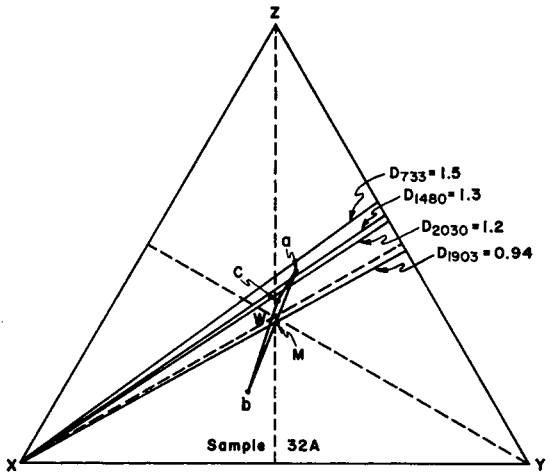

Fig. 7. Comparison of infrared and x-ray data, sample 32A.

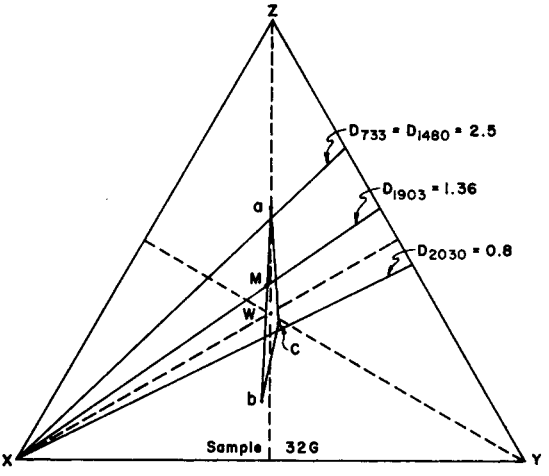

Fig. 8. Comparison of infrared and x-ray data, sample 32G.

Experimental values taken from the graphs yield values of 0.59 and 0.61 for $\cos^2\phi_{M,a}$ for the data of 32A and 32G, respectively. The agreement is surprisingly good, and occurs, incidentally, while the dichroism of the 1903 cm^{-1} band is shifting from 0.94 to 1.36. Using the average value:

$$\cos^2\phi_{M,a} = 0.60 \tag{9}$$

We obtain:

$$\phi_{M,a} = 39° \tag{10}$$

This places **M** close to the (210) normal, since:

$$\phi_{210,a} = 36.8° \tag{11}$$

The proximity of these two vectors is probably fortuitous and is mentioned only to aid in visualizing the position of **M**. The important point is that the dipole moment vector is quite removed from any crystal axis. This tends to limit the usefulness of the 1903 cm^{-1} band for two reasons: (a) it is more profitable to work with bands in which **M** is parallel to one of the crystal axes, and (b) further work would be required to establish precisely the location of **M** for the 1903 cm^{-1} band.

DISCUSSION

Discussion of Morphological Structures

Over the years several simple models have been proposed to explain the texture observed in extruded polymer films. The models may be grouped into three categories and are depicted schematically in Figure 9.

Type I (*a*-axis model) was originally suggested by Holmes et al.[25] The *a* axis is preferentially oriented towards the machine direction. The *b* and *c* axes are randomly distributed in the plane perpendicular to *a*.

Type II (row-orientation model) was suggested by Keller.[26] Numerous crystallites are nucleated along a line parallel to *Z*. Crystals are constrained because of impingement to grow in directions near the *XY* plane, resulting in preferential orientation of *b*, the growth direction, perpendicular to *Z*. The *a* and *c* axes rotate randomly about *b*, resulting in a mild orientation of these two axes parallel to *Z*.

In type III, the crystallite rotates about a particular direction in the *ac* plane of the unit cell, which in turn, is oriented towards *Z*. The *b* axis orients perpendicular to *Z*, while *a* and *c* are tilted at intermediate angles. The screw dislocation structure proposed by Anderson[27] and by Kobayashi[28,29] falls in this category but requires that the axis of crystal rotation should be a simple (*h*0*l*) crystallographic vector, identical in direction with the Burgers vector. This helically wound filament structure is notably similar to the structure of metal whiskers.

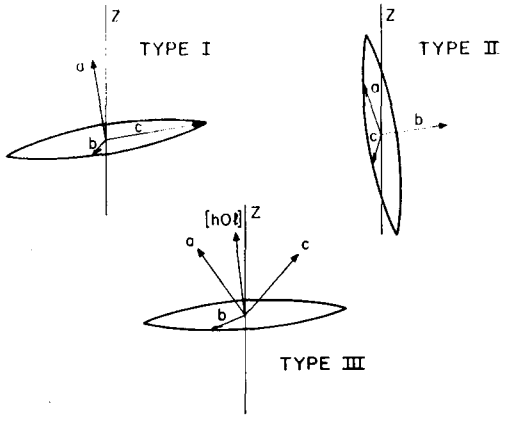

Fig. 9. Three simple morphological models for extruded polyethylene film.

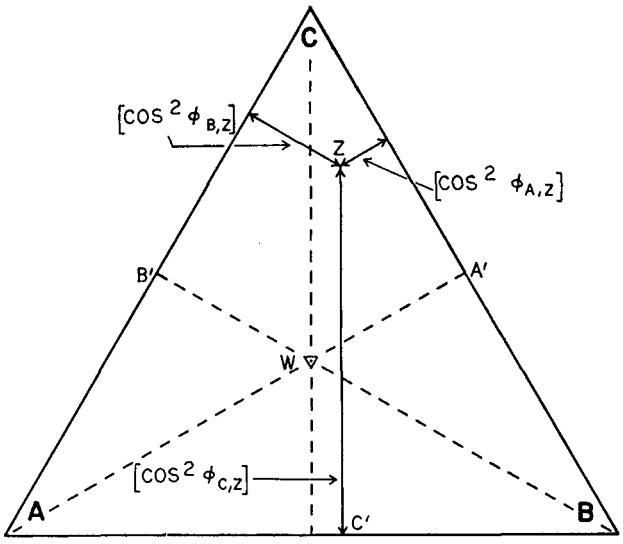

Fig. 10. Definition of the *ABC* orientation function plot.

The data on the blown films may be examined in terms of these three simple models. To do this, we will first introduce the *ABC* orientation function plot. This plot is defined in Figure 10. The quantities $\langle\cos^2\phi_{a,z}\rangle$, $\langle\cos^2\phi_{b,z}\rangle$, and $\langle\cos^2\phi_{c,z}\rangle$ are plotted in an equilateral triangle. Because the crystal axes are orthogonal, only two of the functions are independent, the third being specified by:

$$\langle\cos^2\phi_{a,z}\rangle + \langle\cos^2\phi_{b,z}\rangle + \langle\cos^2\phi_{c,z}\rangle = 1 \tag{12}$$

This plot may be thought of as the inverse of the *XYZ* triangle plot, in analogy with the inverse pole figure.[5] In the *ABC* plot, a single point characterizes the average orientation of the machine direction with respect to the crystallographic axes. The inverse is true in the *XYZ* plot: a single point characterizes the average orientation of a crystallographic direction with respect to the three sample coordinates.

The *ABC* plot is especially useful for indicating the relative degree of *a*-, *b*-, and *c*-axis orientation. The type of behavior predicted for various structures is indicated in Figure 11*a*. The type I model would lie along the line *AW*, indicating parallel orientation of *a* and equal degrees of perpendicular orientation for *b* and *c*. The degree of *a*-axis orientation is indicated by the actual position of the point on *AW*, perfect orientation occurring at *A*. The locus of points for type II is line *BW*, indicating equal degrees of *a* and *c* orientation. Fiber type orientation (*c* oriented towards the fiber axis *Z*, with *a* and *b* random about *c*) would fall along the line *CW*, perfect fiber orientation occurring at *c*.

There is no single line for the type III model. The dotted lines in Figure 11*a* show several possibilities for screw-type structures with rotation about

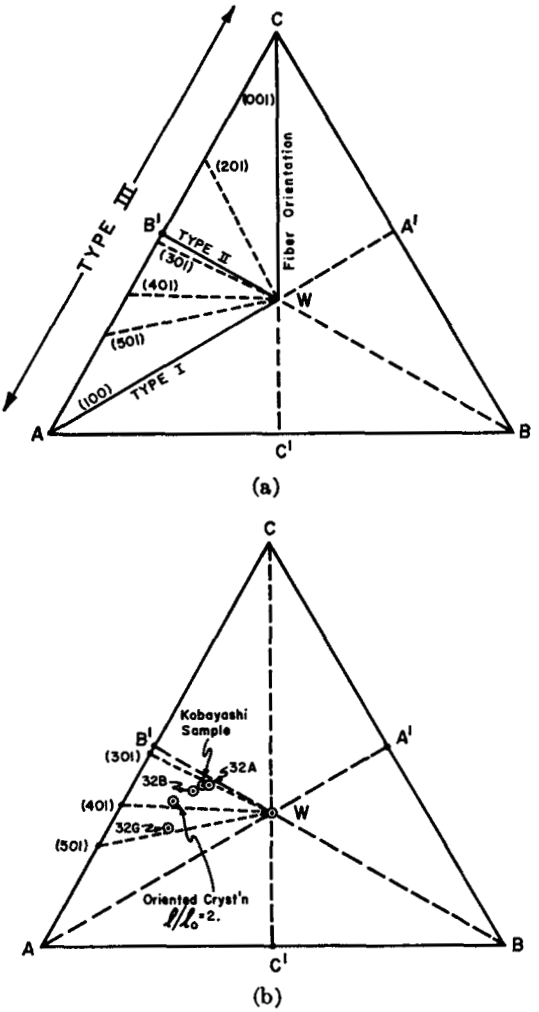

Fig. 11. (*a*) Position of various types of structure on the ABC diagram; (*b*) experimental data for several polyethylene samples.

different (*h*0*l*) vectors. The fiber line *CW* and the type I line *AW* may be thought of as limiting cases of the type III structure, with rotation about (001) and (100) respectively. The type III model allows the relative amount of *a* and *c* axis orientation to vary widely; data for such structures could lie anywhere in the small triangle *AWC*.

Experimental data for several samples is shown in an *ABC* plot in Figure 11*b*. The data for 32A shows nearly equal values of $\langle \cos^2 \phi_{a,z} \rangle$ and $\langle \cos^2 \phi_{c,z} \rangle$ and lies near the type II line. Data for the extruded film supplied by K. Kobayashi lie nearby. Proceeding to extruded film 32G, the degree of *a* axis orientation has increased while the *c* axis orientation has decreased, and the data point is quite a distance from the type II line.

The data point for the laboratory oriented crystallization sample is not as far removed from the type II line as the 32G point.

It is important that one exercise caution in interpreting such a plot. A set of orientation functions does not, in any sense, uniquely determine a structure. This is amply illustrated by the fact that the type II line and the type III line for rotation about (301) are quite close together. Sample 32A and Kobayashi's sample could have either a row orientation structure, a screw dislocation structure, or both. Only negative conclusions can be drawn. For instance, the simple type I and type II structure may be ruled out for sample 32G, as was previously done[6] for the oriented crystallization sample. Evidence of a different nature is required to further define the structure.

Composite Models for Crystal Orientation

In view of recent advances in our knowledge of the oriented crystallization process it is appropriate to examine our data in terms of the more complex structures suggested by these advances. The work of Pennings and Kiel,[30] for instance, suggests a "shish-kebab" structure, consisting of a central fibril of extended chain crystals oriented parallel to the stretch direction covered by an overgrowth of folded-chain fibrils growing in a plane perpendicular to Z. In terms of crystal orientation this structure is a combination of two simple textures, the fiber type and the row orientation type. Depending upon the relative amount of extended and folded chain crystals, the texture can approach either of the two simple models as limiting cases. However, this combination does not appear to be appropriate to explain the unusual orientation in blown film 32G. In the ABC diagram (Fig. 11) a sample possessing combination fiber and row orientation structure must lie in the region bounded by lines WB and WC, which represent the limiting cases. The data points for the oriented recrystallization sample and for 32G are clearly outside this region, as were the data of Judge and Stein[4] for a similar oriented recrystallization sample.

An alternative is to modify the type II structure to allow nonrandom rotation of a and c about b. This idea is put forth by Keller and Machin,[2] combined with extended chain crystals which serve as nuclei. Using this modification, one can explain unequal degrees of a and c axis orientation and even tilting of the a axis at an intermediate angle, as in the films of Holmes and Palmer.

However, a somewhat different structure may also be reconciled with the data. Some recent results by Clough[31] suggest that a spherulitic type of structure may be present in polyethylene crystallized at low orientation. He studied oriented crystallization of crosslinked polyethylene in the range 20–50% elongation. In this region, spherulitic structures formed which were large enough to observe on the polarizing microscope. The extinction patterns indicated that different structures are present in different sectors within an individual spherulite, which may thus be termed a "composite

TABLE V
Summary of Clough's Results on Orientation-Grown Spherulites

Reference	Local anisotropy ($n_R - n_T$)		Film birefringence ($n_Z - n_y$)
	Polar	Equatorial	
26	Very slightly (−)	Strongly (−)	+
27	Strongly (−)	Moderately (−)	−

spherulite." The equatorial regions (perpendicular to the stretch direction) showed the usual high negative anisotropy observed in isotropically grown spherulites. In the polar regions, however, the optical anisotropy was only slightly negative, and the material was nearly nonbirefringent. In later experiments Clough[32] observed orientation-grown spherulites in which the reverse was found—the polar regions exhibited a higher negative anisotropy than the equatorial regions. The overall film birefringence was positive in the first sample and negative in the second, as one would predict from the microscopic observations. These results are summarized in Table V.

These results, which will be reported at a later date, are mentioned because of certain similarities with the observed data on extruded films. First of all, the light-scattering data on the extruded films suggest the existence of aggregates with roughly equal dimensions in the machine and transverse directions. Such is also the case in the orientation grown spherulites. Moreover, films of both positive and negative birefringence are observed in both cases. We may explain the crystal orientation data as follows: in 32A, the equatorial regions are type II and the polar regions are type III, with rotation about (301). This gives equal degrees of a and c axis orientation as observed. In 32G, the equatorial material is still type II, but in the polar regions, the type III material which occurs places the a axis closer to a radial position. This results in increasing a axis orientation parallel to the machine direction. These are presented as tentative conclusions, since it is recognized that measurement of crystal orientation does not define the morphology.

Growth of Composite Spherulitic Structures

A model for the structure of orientation-grown spherulites is shown in Figure 12. The spherulite is a composite of two simple structures: the type II structure in the equatorial regions and a type III structure in the polar regions. This combination places b approximately perpendicular to Z in both regions. The structure, once nucleated, tends to grow in all directions, growth being halted by impingment upon another growing spherulite. Thus the final shape of the spherulites will be dependent upon the placement of the primary nuclei. One limiting case is Keller's row orientation structure, which occurs when nuclei are closely spaced in the Z direction but are more widely spaced in the X and Y directions. Another

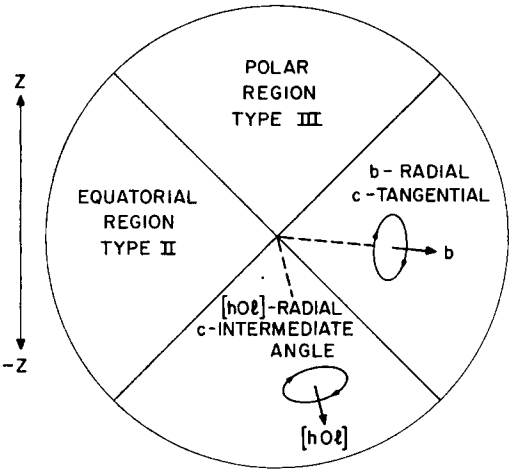

Fig. 12. Composite structure in anisotropically grown polyethylene spherulites.

limiting case occurs when nuclei tend to lie close together in the same XY plane, but are more widely spaced in the Z direction. This results in a sample composed entirely of type III material, and could be explanation for the orientation observed by Holmes and Palmer.[8]

It is important to remember that these two structures are limiting cases which may not be realized in a given sample. In Clough's spherulitic samples the nucleation was apparently isotropic, meaning that, on the average, nuclei were somewhat equally spaced in all directions. This is indicated by the observation that the spherulites are approximately spherical. The pattern of placement of the primary nuclei will be vitally important in determining the shape of the resulting spherulite, for this pattern will govern the average distance a spherulite can grow in a given direction before impingement occurs. This average distance could be angularly dependent. Keller's row orientation structure assumes, for example, that nuclei are closely spaced along the Z direction but widely spaced along X and Y. This results in suppression of the polar region growth. In other samples, however, different patterns of primary nuclei may occur, resulting in variation in the relative amount of polar and equatorial material. Also, by varying the sign and magnitude of the optical anisotropy of the two regions as well as the relative abundance of polar and equatorial material, one can explain variation in the sign and magnitude of the overall birefringence of the sample, and in the degree of orientation of the three crystallographic axes. Changes in the a and c axis orientation functions, in the birefringence, and in the infrared dichroism, could be brought about within this series of films by shifts in the average a and c axis tilt angles in the polar regions, the a axis shifting closer to the radius (machine direction) for 32G and for 32A. These changes occur at a nearly constant degree of b axis orientation. Still other samples might exhibit the pure "row orientation" structure, for which there is ample evidence in the literature. However, it

would seem reasonable that a certain minimum orientation might be required to produce the pure row orientation structure, and that below this limit the growth of polar regions must also be considered. Further studies of oriented crystallization, especially in the low orientation region, are clearly indicated.

Impact Strength of Blown Films

The impact strengths of the blown films were measured in the Monsanto Laboratories by the "drop dart" method.[33] In this method, the film is clamped in a horizontal frame and a dart is dropped onto the film from a fixed height. The weight of the dart may be increased by adding weights. For every dart weight, a number of tests are made, and the fraction of the tests in which the film broke is recorded. The weight for which failure occurs in 50% of the tests is taken as a measure of impact strength. Naturally, the results are comparable only when the film thickness is held fairly constant, as was done in this series of samples. The results, reported in Table VI, show a monotonic increase in impact strength from 32A to 32G. The overall improvement in impact strength is a factor of 2.5 in W_{50}, the dart weight for 50% probability of failure.

TABLE VI
Impact Strength by the Drop Dart Method

Sample	W_{50}, g[a]
32A	83
32B	107
32C	113
32D	147
32E	172
32F	193
32G	205

[a] Dart weight which will break the film in 50% of the trials. Values are comparable only if the film thickness is held constant, as was done here.

The change in impact strength is possibly related to the change in the domain structure, or state of crystal aggregation, as revealed by light scattering. The impact strength can also be correlated with the degree of orientation as measured by x-ray diffraction or dichroism. However, when several structural factors are changing simultaneously, it is difficult to determine which is responsible for the improved impact.

Clegg and Huck[34] found that impact strength does not necessarily correlate with the birefringence Δ_z. One factor which may have a strong influence on impact strength is the occurrence of transcrystallization. Those samples with poorest impact strength are the ones for which transcrystallization is most prevalent. As one proceeds from 32A to 32G, the b axis maximum in the normal direction decreases and vanishes, indicating a corresponding decrease in the thickness of the transcrystalline skin. This

coincides with increasing cooling air velocities and better impact strength. Clegg and Huck also observed that surface crystallization decreased with more rapid quenching, as we observe here. Such a skin is probably a source of weakness for the polymer film for two reasons.

(*a*) The structure at the surface and at the interior of the sample will be different, so the surface will fail at a different (possibly lower) strain than the interior material. The surface material will rupture before the interior material is supporting its share of the load, because of the different load/elongation relationships in the two regions.

(*b*) The transcrystalline layer may have a number of flaw lines extending from the surface into the interior and serve as convenient avenues of crack propagation. Such flaw lines would be the likely result of the parallel growth of lamellae in the film normal direction.

We might ask why the transcrystalline layer is favored by low quench rates and suppressed by rapid quenching. This is probably due to kinetic considerations. Two competing processes, transcrystallization and interior nucleation, can occur. However, the transcrystallization is limited by the crystal growth rate. If the material is quenched rapidly, the transcrystalline front cannot propagate very far into the polymer before a large undercooling is achieved, which would cause the interior to nucleate independent of the surface layer. The result is a thinner surface skin at higher quenching rates.

This paper is based in part upon a thesis submitted by C. Richard Desper in partial fulfillment of the requirements for the degree of Doctor of Philosophy at the University of Massachusetts, Amherst, Massachusetts. The author also wishes to acknowledge the support of the Office of Naval Research and the Petroleum Research Fund.

This paper reports research undertaken at the US Army Natick (Mass.) Laboratories and has been assigned No. TP 416 in the series of papers approved for publication. The findings in this report are not to be construed as an official Department of the Army position.

References

1. P. H. Lindenmeyer and S. Lustig, *J. Appl. Polym. Sci.*, **9**, 227 (1965).
2. A. Keller and M. J. Machin, *J. Macromol. Sci.*, **B1**, 41 (1967).
3. T. T. Li, R. J. Volungis, and R. S. Stein, *J. Polym. Sci.*, **20**, 199 (1956).
4. J. T. Judge and R. S. Stein, *J. Appl. Phys.*, **32**, 2357 (1961).
5. W. R. Krigbaum and R. J. Roe, *J. Chem. Phys.*, **41**, 737 (1964).
6. C. R. Desper and R. S. Stein, *J. Appl. Phys.*, **37**, 3990 (1966).
7. R. Kitamaru, H. D. Chu, and W. Tsuji, *J. Polym. Sci. B*, **5**, 237 (1967).
8. D. R. Holmes and R. P. Palmer, *J. Polym. Sci.*, **31**, 345 (1958).
9. R. S. Stein and T. Hotta, *J. Appl. Phys.*, **35**, 2237 (1964).
10. J. L. Matthews, H. S. Peiser, and R. B. Richards, *Acta Cryst.*, **2**, 85 (1949).
11. P. L. Clegg and N. D. Huck, *Plastics* (London), **26**, No. 283, 107 (1961).
12. R. K. Eby, *J. Appl. Phys.*, **35**, 2720 (1964).
13. Y. Ito, *Kobunshi Kagaku*, **18**, 228 (1961).
14. R. S. Stein, *J. Polym. Sci.*, **24**, 383 (1957).
15. C. R. Desper, Ph.D. Thesis, Dept. of Chemistry, Univ. of Mass., Amherst, Mass., 1967, p. 171.
16. S. Krimm, C. Y. Liang, and G. B. B. M. Sutherland, *J. Chem. Phys.*, **25**, 549 (1956).

17. R. S. Stein and G. B. B. M. Sutherland, *J. Chem. Phys.*, **21**, 370 (1953).
18. T. Okada and L. Mandelkern, *J. Polym. Sci. A-2*, **5**, 239 (1967).
19. J. L. Koenig, S. W. Cornell, and D. E. Witenhafer, *J. Polym. Sci. A-2*, **5**, 301 (1967).
20. J. R. Nielsen and R. F. Holland, *J. Mol. Spectr.*, **4**, 488 (1960).
21. B. E. Read and R. S. Stein, ONR Technical Report No. 93, Dept. of Chemistry, Univ. of Mass., Amherst, Mass., 1967.
22. C. R. Desper, *J. Polym. Sci. A-2*, **6**, 1203 (1968).
23. S. L. Aggarwal, G. P. Tilley, and O. J. Sweeting, *J. Appl. Polym. Sci.*, **1**, 91 (1959).
24. A. Keller and I. Sandeman, *J. Polym. Sci.*, **15**, 133 (1955).
25. D. R. Holmes, R. G. Miller, R. P. Palmer, and C. W. Bunn, *Nature*, **171**, 1104 (1953).
26. A. Keller, *Nature*, **174**, 926 (1954).
27. F. R. Anderson, *J. Polym. Sci. B*, **3**, 721 (1965).
28. K. Kobayashi, in *Polymer Single Crystals*, P. H. Geil, Ed., Interscience, New York, 1963, pp. 465–475.
29. K. Kobayashi and T. Nagasawa, private communication.
30. A. J. Pennings and A. M. Kiel, *Kolloid-Z.*, **205**, 160 (1965).
31. S. B. Clough, Ph.D. thesis, Dept. of Chemistry, Univ. of Mass., Amherst, Mass., 1966.
32. S. B. Clough, private communication.
33. R. M. Supnick and C. M. Adams, *Plastics Technol.*, **2**, 151 (1956).
34. P. L. Clegg and N. D. Huck, *Plastics* (London), **26**, No. 282, 114 (1961).

Received October 19, 1967
Revised August 14, 1968